Received: 1 June 2020 | Revised: 30 October 2020 | Accepted: 10 November 2020

DOI: 10.1002/jbm.b.34761

Society For Biomaterials | WILEY

ORIGINAL RESEARCH REPORT

3D-printed cryomilled poly(ε-caprolactone)/graphene composite scaffolds for bone tissue regeneration

Daniela Dias[1,2] | Ana C. Vale[1,2] | Eunice P. F. Cunha[3] | Maria C. Paiva[3] | Rui L. Reis[1,2] | Cedryck Vaquette[4] | Natália M. Alves[1,2]

[1]3Bs Research Group, I3Bs – Research Institute on Biomaterials, Biodegradables and Biomimetics, University of Minho, Headquarters of the European Institute of Excellence on Tissue Engineering and Regenerative Medicine, Guimarães, Portugal

[2]ICVS/3B's, PT Associate Laboratory, Guimarães, Portugal

[3]Institute for Polymers and Composites, Department of Polymer Engineering, University of Minho, Guimarães, Portugal

[4]Institute of Health and Biomedical Innovation, Queensland University of Technology, Brisbane, Australia

Correspondence
Cedryck Vaquette, Institute of Health and Biomedical Innovation, Queensland University of Technology, Cnr Blamey Street & Musk Avenue, Kelvin Grove, Brisbane, QLD 4059, Australia.
Email: c.vaquette@uq.edu.au

Natália N. Alves, I3Bs – Research Institute on Biomaterials, Biodegradables and Biomimetics, University of Minho, Headquarters of the European Institute of Excellence on Tissue Engineering and Regenerative Medicine, Avepark, 4805-017 Barco, Guimarães, Portugal.
Email: nalves@i3bs.uminho.pt

Funding information
Education, Audiovisual and Culture Executive Agency, Grant/Award Number: ICI-ECP Education Cooperation Programme (388414-EM; European Regional Development Fund, Grant/Award Numbers: LA ICVS/3Bs - 2015-2017, UID/CTM/50025/2013, UID/CTM/50025/2016; Fundação para a Ciência e a Tecnologia, Grant/Award Number: SFRH/BD/87214/2012

Abstract

In this study, composite scaffolds based on poly(caprolactone) (PCL) and non-covalently functionalized few-layer graphene (FLG) were manufactured by an extrusion-based system for the first time. For that, functionalized FLG powder was obtained through the evaporation of a functionalized FLG aqueous suspension prepared from a graphite precursor. Cryomilling was shown to be an efficient mixing method, producing a homogeneous dispersion of FLG particles onto the PCL polymeric matrix. Thereafter, fused deposition modeling (FDM) was used to print 3D scaffolds and their morphology, thermal, biodegradability, mechanical, and cytotoxicity properties were analysed. The presence of functionalized FLG demonstrated to induce slight changes in the microstructure of the scaffold, did not affect the thermal stability and enhanced significantly the compressive modulus. The composite scaffolds presented a porosity of around 40% and a mean pore size in the range of 300 μm. The cell viability and proliferation of SaOs-2 cells were assessed and the results showed good cell viability and long-term proliferation onto produced composite scaffolds. Therefore, these new FLG/PCL scaffolds comprised adequate morphological, thermal, mechanical, and biological properties to be used in bone tissue regeneration.

KEYWORDS
3D printing, bone tissue regeneration, composite scaffold, functionalized few-layer graphene, polycaprolactone

1 | INTRODUCTION

Recently 3D printing techniques provided new approaches for the fabrication of biomedical structures, offering the possibility to precisely control the geometry and size of the structures.[1] Fibers, scaffolds and other complex structures with varied geometries are some of the examples of what can be obtained by 3D printing.[2] Fused deposition modeling (FDM) is one of the fabrication methods available for the production of three-dimensional structures, enabling the extrusion of thermoplastic material through an extrusion nozzle in a layer-by-layer way.[3] FDM comprises the simplicity and flexibility in material handling and processing, being a highly reproducible method,

Daniela Dias and Ana C. Vale contributed equally (co-first authors).

with a relatively moderate speed, which allows control over the major physical characteristics of the resulting scaffolds, like mechanical properties, porosity and pore shape.[4]

The combination of two or more materials with different compositions and properties can result in composites with tunable physical and chemical characteristics, and increased mechanical properties or bioactivity.[5] Composite materials are used in different applications due to their enhanced capabilities.[6] In the past few years, polymer-based composites have emerged owing to their enhanced toughness and diversity of processing methods. Regarding scaffolds for bone regeneration, different biodegradable polymers have been recognized as potential candidates, for instance, polycaprolactone (PCL), polylactic acid (PLA), and also natural polymers such as chitosan and collagen.[7] Depending on the processing method, those structures may present highly tunable mechanical properties, porosity and degradation rate. Furthermore, some of the polymeric materials enable scaffolds to be loaded with osteoinductive proteins or osteogenic cells, to better mimic native tissues.[8] PCL is an aliphatic polyester approved by the Food and Drug Administration, being considered as a soft- and hard-tissue-compatible bioresorbable material.[9] However, disadvantages such as its poor hydrophilicity and low degradation rate can reduce its biological performance.[10] A good strategy to improve its performance could be the incorporation of another material as a filler, like few-layer graphene (FLG).[11]

Graphene is a planar sheet of sp^2 hybridized carbon atoms densely arranged into a 2D hexagonal lattice.[12] Its great properties have been a point of interest to many researchers. Graphene is difficult to obtain in large amounts as a bulk material, however FLG, which is formed by flakes with stacks of a few graphene layers (up to 10 maximum), can be produced by exfoliation of graphite. Graphene presents a high elastic modulus (≈1TPa), a tensile strength of 130 ± 10 GPa,[13,14] presents a high thermal conductivity, above 3,000 W mK^{-1}, and a large theoretical specific area of 2,630 m^2 g^{-1} and can sustain extremely high electric current densities.[15,16] FLG properties are close to those of graphene, being an excellent reinforcement material for the preparation of polymer composites.[17] Besides, FLG can interact with other biomolecules such as DNA, enzymes, proteins, or peptides for regenerative medicine and tissue engineering. These bioactive compounds can be used as functionalization agents via physical adsorption.[15] The functionalization is usually carried out to increase biocompatibility and, in many cases, the hydrophilicity of the FLG forms.[18] The functionalization can be achieved either by covalent[19] or non-covalent binding of a variety of chemical moieties.[20] Non-covalent functionalization is an attractive method based on hydrophobic interactions with amphiphilic molecules, offering the possibility of attaching functional groups to FLG without disturbing its electronic network.[21] It should be mentioned that non-covalent functionalization of graphite with specific amphiphilic molecules is frequently used to achieve its liquid phase exfoliation (LPE) in water and form FLG suspensions. Water is a preferred solvent for the preparation of materials for biomedical applications, however its high surface tension and polar nature hampers the interaction with graphene and the ability to form stable suspensions. The LPE of graphite into FLG can be achieved in aqueous solutions of amphiphilic molecules that strongly interact with water through their polar moiety and with graphene through their non-polar moiety. These molecules adsorb at the graphene surface preventing its re-staking and allowing solvation of the FLG flakes. Typically, amino-pyrene, aminomethyl pyrene, pyrene carboxylic acid, pyrene butyric acid and pyrene sulfonic acid derivatives have been used in the graphite exfoliation process at concentrations that range from 0.1 to 10 mM. In this work, an aqueous solution with 0.05 mM of functionalized pyrene containing a carboxyl group (PY) was used (Figure S1). PY was prepared following a synthetic procedure developed previously.[22] This approach was used aiming at two goals: first, to produce FLG by exfoliation of the graphite nanoplatelets in water; second, after drying the PY-functionalized FLG, to disperse it in PCL by melt mixing, to produce a composite material with enhanced interfacial bonding. In this study, PCL and FLG were blended for the first time to obtain FDM-based 3D-printed composite scaffolds. To achieve that, it was necessary to homogeneously mix PCL with FLG ensuring a good dispersion of the FLG particles onto the polymeric matrix. Herein, a solvent-free blending technique was used, the cryomilling, which is an environmentally friendly and versatile approach for processing materials in their dry state used to prepare polymer composites with a high degree of filler dispersion.[23] This work investigated the use of an extrusion-based 3D printing system to produce new PCL scaffolds reinforced with a functionalized FLG, fG(Micrograf), and also, the influence of the FLG reinforcement on the scaffolds microstructural, mechanical and cellular behavior properties, envisaging bone tissue regeneration applications.

2 | MATERIALS AND METHODS

2.1 | Materials

Micrograf® HC11, was provided by Nacional de Grafite, Ltda (Brazil) and it is a micronized graphite, with 99.5% purity and an average particle diameter (d50) of 11 μm. The few-layer graphene (FLG) obtained from the previous pristine material will be designated by fG(Micrograf), which was obtained by exfoliation of graphite in the form of a stable FLG suspension. Non-covalent functionalization of the graphite was performed using a pyrene derivative (PY) with amide and carboxylic groups presented in Figure S1, (Z)-4-oxo-4-(pyren-1-ylamino)but-2-enoic acid, which was synthesized following the protocol optimized by our group.[13] This pyrene derivative soluble in water was chosen since it showed to be effective in the exfoliation and stabilization of graphene nanoplatelets in aqueous media. Medical grade polycaprolactone (Mn = 80 kDa, Mw/Mn < 2) was purchased from Sigma-Aldrich (Australia). Before its use for the fabrication of the scaffolds, PCL was blended with fG(Micrograf) through the cryomilling technique.

2.2 | Production and characterization of functionalized FLG suspension

The production of a homogeneous suspension of fG(Micrograf) was carried out by stabilizer-assisted liquid-phase exfoliation of Micrograf, a non-covalent approach using PY as a stabilizer, in an aqueous solution. Briefly, a 5 x 10^{-5} M PY solution was prepared at pH 7 and

under sonication until the total dissolution of PY. Then, 250 mg of Micrograf was added to this solution to form a 0.5 mg mL^{-1} suspension by sonication for 4 hr. The forces applied through cavitation effects enhanced the dispersion of the graphite agglomerates and their exfoliation, increasing the surface of FLG available for adsorption of PY molecules via π-π interactions.[24]

Raman spectroscopy analysis was performed on a LabRAM HR Evolution Raman Microscope (Horiba Scientific, Japan) using a 532 nm laser and the results were analysed using the LabSpec6 software. The pristine Micrograf and fG(Micrograf) solutions were sprayed on a glass slide, positioned on a heating plate for faster water evaporation and deposition of the FLG, and analysed. The thermal stability of fG(Micrograf) was evaluated by thermogravimetric analysis, TGA, performed on a TA Q500 equipment (TA Instruments, USA), and all measurements were carried out under a nitrogen atmosphere, heating from 40 to 900°C at a rate of 10°C min^{-1}. Finally, the FLG flakes were observed by scanning transmission electron microscopy (STEM) on a NanoSEM FEI Nova 200 microscope operating at 15 kV accelerating voltage.

2.3 | Fabrication of 3D-printed scaffolds

Firstly, the composite powder was produced by cryomilling, providing a homogeneous mixture of PCL powder with FLG. The FLG powder was obtained from the fG(Micrograf) suspension, which was dried in the oven at 90°C for approximately 1 day. Then, PCL and FLG powders were properly cryomilled in a 6,770 SPEX Freezer/mill resulting in a composite powder of PCL and 0.5 wt% of fG(Micrograf). The choice of 0.5 wt% filler content in the composite was based on several previous studies that reported successful composite scaffold production and good cellular behavior with this graphene content.[25-29]

Based on previous studies to mitigate possible re-agglomeration effects during the freezing step of the cryomilling process,[30] a protocol was implemented based on 10 min pre-cooling in liquid nitrogen and 20 min of continuous milling per cycle. After this procedure, the composite powder was collected and kept in a sealed container, ready for 3D printing.

The production of 3D-printed scaffolds was carried out on a Bio-Extruder system developed at the Polytechnic Institute of Leiria (I.P.L., Portugal), which is a melt extrusion-based additive manufacturing process with controlled internal/external geometry suitable for tissue engineering applications, as described by Domingos et al.[2,31,32] Control and composite scaffolds were fabricated using the same process parameters to focus the analysis on the effects of graphene incorporation. Briefly, PCL ground pellets and cryomilled composite powder were melted in a reservoir (155°C), forced with pressurized air into a single-screw extruder, and printed at 155°C in a 0°/90° lay-down pattern with fiber spacing of 0.75 mm through a 22G nozzle. The deposition rate and translational collector speed were adjusted in order to achieve continuous and stable printing conditions. The produced scaffolds presented a honeycomb-like structure of fully interconnected square pores, which were cut in cylinders with 5 mm diameter and, before cellular tests, sterilized through ethylene oxide (EO) exposure (42°C, 3 hr).

2.4 | Thermal analysis

Differential scanning calorimetry (DSC) was used to evaluate the melting temperature (T_m), melting enthalpy (ΔH), and crystallinity degree (χ_C) of PCL and PCL + fG(Micrograf) scaffolds. The analysis was carried out on a DSC131 evo (SETARAM instrumentation, France), all the experiments were conducted at a constant heating/cooling rate of 10°C min^{-1} under a nitrogen flow. The analysis was programmed in two stages: heating the sample to 100°C and keeping under isothermal conditions for 5 min to erase any prior thermal history; then, cooling to 0°C and finally, reheating to 100°C. The same procedure was carried out on the control scaffolds of neat PCL. T_m and ΔH of PCL were determined from the first and the second heating scans. χ_C was calculated by applying the following Equation (1):

$$\chi_C = \frac{\Delta H}{\Delta H_u^\circ} w, \quad (1)$$

where ΔH^0_u is the melting enthalpy of 100% crystalline PCL, that is, 166 J g^{-1}, and w is the weight fraction of PCL in the composite.[33]

In order to estimate the amount of FLG incorporated in the composite scaffolds, thermogravimetric analysis, TGA, was performed using a TA Q500 equipment (TA Instruments, USA) under a nitrogen atmosphere, heating at 10°C min^{-1} in the temperature range from 40 to 900°C. At least three measurements were carried out for each sample.

2.5 | Microstructural analysis

Firstly, the morphological analysis of the scaffolds produced was carried out using a JSM-6010LV scanning electron microscope (JEOL, Japan) operating at 15 kV accelerating voltage. The fibers deposited layer was observed as well as its cross-section. For the cross-section preparation, the scaffolds were immersed in liquid nitrogen for 5 min and sectioned with a sharp razor blade. Immediately before SEM observation, the samples were coated with a thin gold layer.

In addition, to evaluate alterations in the 3D microstructure of the scaffold during the accelerated degradation test, a high-resolution μCT Skyscan 1072 scanner (Skyscan, Kontich, Belgium) was used to scan scaffolds with a pixel size of 11 μm and the X-ray source adjusted at 43 keV of energy and 230 μA of current. Data acquisition (SkyScan 1072), data reconstruction (NRecon, SkyScan), and data analysis (CTAn, SkyScan) software were used for image processing in CT reconstructions, and to create and visualize the reconstructed microstructures. Three-dimensional images of the scaffold's structure were obtained and the main microstructural parameters were determined, the porosity, the mean pore size, and the mean wall thickness.

2.6 | Accelerated degradation

Since PCL is a semi-crystalline bioresorbable synthetic polymer belonging to the aliphatic polyester family, and it is known to have a very slow degradation rate of up to 4 years in certain conditions.[34] As so, to assess the weight loss of the produced scaffolds within a shorter time scale, an accelerated hydrolytic degradation study was performed based on the protocol proposed by Lam et al.,[34,35] using a basic medium (5 M NaOH), which would enhance the hydrolysis of polyesters. Composite and control scaffolds with 5 mm diameter and 3 mm height were immersed in the basic solution during 7, 14, 21, and 28 days. The scaffolds were kept in tubes with their screw-caps tightened according to the time points in a 37°C incubator. The samples were removed after weekly time points, rinsed thoroughly with osmotized water, and dried in the oven for 12 hr at 35°C. Finally, the samples were kept for further analysis. At least three samples were used for each time point. The weight loss from each scaffold was determined using Equation (2).

$$\textit{weight loss}\,(\%) = \frac{w_i - w_f}{w_i} \times 100, \qquad (2)$$

where W_i and W_f are, respectively, the initial dry weight and the final dry weight of the sample. Each experiment was repeated three times and the average value was taken as the weight loss. The sample morphology was analysed through SEM and μCT.

2.7 | Mechanical analysis

In order to investigate FLG's addition effect on the mechanical properties of the 3D printed scaffolds, compression and tensile tests were performed. For the compression tests, the samples were cut into 5 mm diameter and 3 mm thick cylinders. The produced scaffolds were tested on an universal mechanical testing equipment (INSTRON 5540) using a 1 kN load cell. Each specimen was compressed to a strain of approximately 50% at a rate of 1 mm.min^{-1}. The compressive elastic modulus was determined from the linear region of the compressive stress–strain curve (from 0 to 0.1% strain). At least five samples of PCL and composite scaffolds were analysed. For the tensile tests, the specimens were cut into a rectangular shape (5 x 40 mm^2). The produced scaffolds were tested on the INSTRON equipment, using a 1 kN load cell, a speed of 1 mm min^{-1}, and a gauge length of 20 mm. At least five samples were tested for both scaffold conditions to obtain the mean and standard deviation values for each mechanical parameter.

2.8 | In vitro cellular tests

Envisaging orthopedic applications, the human osteosarcoma cell line SaOs-2 obtained from the European Collection of Cell Cultures (ECCC, UK), which presents an osteoblastic phenotype, was used for the in vitro experiments. Briefly, SaOs-2 were cultured in a low glucose Dulbecco's modified minimum essential medium (DMEM) with phenol red and supplemented with sodium bicarbonate, 10% FBS and 1% penicillin–streptomycin (pH 7.4), and then, incubated at 37°C in a humidified air atmosphere of 5% CO_2. After trypsinization, SaOs-2 were seeded onto the surface of scaffolds cut in cylinders (5 mm diameter and 1 mm height), which were cultured during different time points (1, 3, 7, 14, and) to quantify the osteoblastic bone formation and the cell proliferation on the material. Per condition, three scaffolds were studied using non-adherent 24 well plates and 1.5 ml of the cell suspension (3.3 x 10^4 cells mL^{-1}) was seeded onto each sample. Plates were incubated at 37°C in a humidified air atmosphere of 5% CO_2, and the medium was replaced every 2–3 days.

The osteoblastic bone formation was assessed through the quantification of alkaline phosphatase, the most frequently used biochemical marker since its expression can be a strong indicator of osteoblast's presence in culture. Therefore, ALP quantification was performed in lysed cells at days 1, 3, 7, and 14. After each incubation period, cells that grow and proliferate into each sample were lysed by osmotic (by adding ultrapure water) and thermal shock (firstly with a water bath at 37°C for 1 hr, and then, by ultra-freezing at −80°C at least 1 hr before use). The obtained supernatant was analysed by measuring the ALP expression following the *p*-nitrophenol assay (Sigma). Briefly, all samples were defrosted and adequately prepared (avoiding the light), to obtain their absorbance values at 405 nm. The ALP amounts were calculated using a standard curve previously obtained with the ALP standards freshly prepared.

To investigate the cell proliferation into the produced scaffolds, the quantification of double-stranded DNA (dsDNA) was made for all culturing period of cells tested (1, 3, 7, and 14 days). Initially, cells were lysed and the obtained supernatant was analysed using the PicoGreen dsDNA kit (Life Technologies, UK). The recovered supernatant was carefully read (avoiding the light) on a microplate reader (Biotek, USA) using 485 and 528 nm as excitation and emission wavelengths, respectively. The DNA amounts were calculated using a standard curve previously obtained. For all cellular tests, at least three triplicates were used for each condition.

2.9 | Statistical analysis

Some experimental results were presented as mean ± standard deviation based, at least, in three replicates (n = 3). Statistical significance between groups was determined by two-way ANOVA with Tukey's Multiple comparison test, using GraphPad Prism version 6.0 (GraphPad software, San Diego, CA). Statistical differences were represented and set to $p < .01$(**), $p < .001$(***), and $p < .0001$(****).

3 | RESULTS

3.1 | Production and characterization of functionalized FLG suspension

Figure 1 presents the Raman spectra of pristine Micrograf, and fG(Micrograf), and both spectra exhibit the three characteristic bands

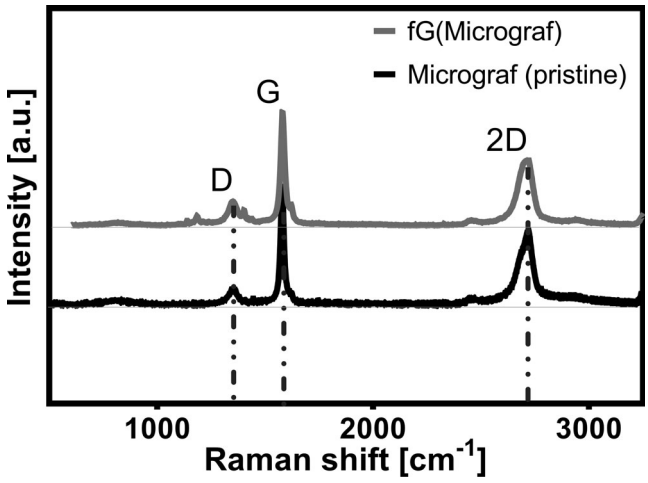

FIGURE 1 Raman spectra of Micrograf (pristine), and fG(Micrograf)

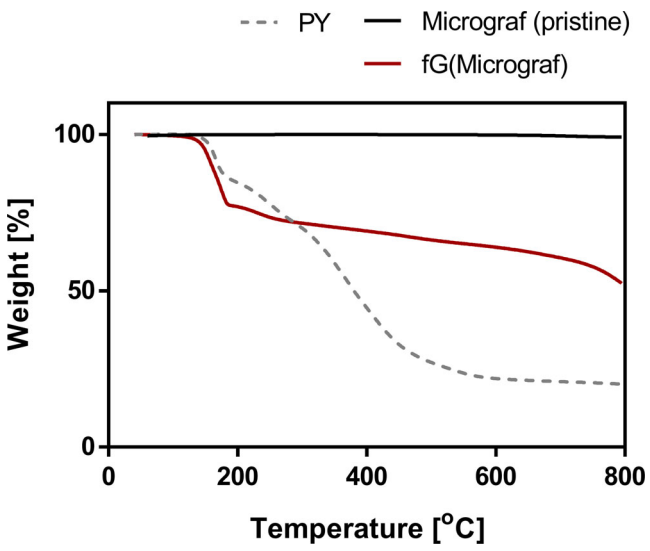

FIGURE 2 TGA thermographs of PY, Micrograf (pristine), and fG(Micrograf)

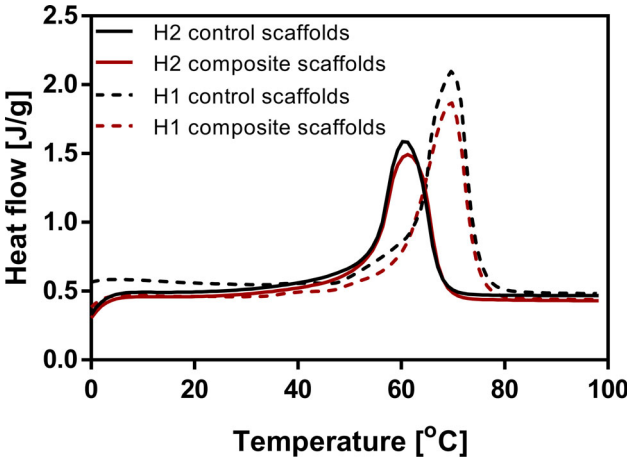

FIGURE 3 DSC first (H1) and second (H2) heating scans for control (PCL) and composite (PCL + fG(Micrograf)) scaffolds

of graphite-based carbon materials (D, G, and 2D). The D band is positioned near 1,342 cm^{-1} and is due to the presence of defects in the hexagonal sp^2 carbon lattice of FLG. The G band is located near 1,580 cm^{-1} and results from in-plane vibrations of the ordered sp^2 bonded carbon hexagonal lattice.[36] The intensity ratio between D and G peaks (I_D/I_G) has been used as an indicator of the increase in disorder of FLG structure caused by covalent chemical modification, ripples, edges, and charged impurities.[37] The 2D band, near 2,700 cm^{-1}, has approximately the double frequency of the D band and results from the second-order Raman scattering.[38] This peak may be used to determine the number of stacked layers (up to 5) in n-layer FLG, by the analysis of its shape, width, and position of the 2D band. Regarding pristine graphite, the 2D band appears at approximately 2,720 cm^{-1} and consists of two components,[39] while in graphene it is observed as a single sharp peak.[40]

The functionalization of Micrograf with PY was studied by TGA, comparing the weight losses of PY, Micrograf and fG(Micrograf) powders heated under nitrogen, as represented in Figure 2. The TGA results show that PY alone presented the lowest thermal stability, starting a thermal degradation process at approximately 150°C. Micrograf is thermally stable under the test conditions and does not show evidence of thermal degradation. After functionalization with PY, the onset of thermal degradation is observed at approximately 150°C, with a major weight loss below 200°C in close resemblance with PY, demonstrating the functionalization of FLG with PY.

Additionally, STEM was used to image the FLG obtained after the functionalization process, and, as Figure S2 shows, a flake of fG(Micrograf) can reach tens of micrometers.

3.2 | Thermal analysis

DSC analysis was conducted on the composite scaffolds to study the influence of FLG presence on the crystallization kinetics of PCL. The DSC curves for the first (H1) and second (H2) heating cycles of PCL and PCL + fG(Micrograf) scaffolds are shown in Figure 3. The melting temperature (T_m), the melting enthalpy (ΔH), and the crystallinity degree (χ_C) for PCL and PCL + fG(Micrograf) scaffolds regarding the two scans are presented in Table 1.

Attending to the results presented in Figure 3 and Table 1, no significant changes are observed between control and composite scaffolds for both heating scans, meaning that the FLG incorporation did not affect the melting transition of PCL in the scaffolds. The first heating stage provides the melting temperature and crystallinity of the as-produced PCL scaffolds. Higher values of Tm, ΔH, and χ_C were obtained for the as-produced composite structures, when compared to the results obtained for the second heating scan, after erasing the thermal history of the PCL and cooling under controlled conditions.

TGA analysis was performed to evaluate the thermal stability and FLG weight composition of the produced scaffolds. The TGA curves

shown in Figure 4 demonstrate that both control and composite scaffolds present similar thermal stability when heated up to 900°C under an inert atmosphere, which means that the incorporation of 0.5 wt% of fG(Micrograf) did not affect the thermal stability of the scaffolds.

For both cases, the major weight loss happened between 350 and 450°C, due to the decomposition of PCL. Above 450°C, the weight loss stabilized for both control and composite scaffolds. However, a higher residual weight was noted for the composite scaffolds due to the presence of fG(Micrograf), consistent with the incorporation of 0.5 wt% of reinforcing material.

3.3 | Microstructural analysis

The surface topography of the scaffolds was assessed using SEM. Figure 5a shows its surface morphology, Figure 5b represents their cross-section and Figure 5c illustrates the macroscopic aspect of the printed scaffolds. Noticeably, the PCL fibers form a regular cross-section of circular shape when compared to PCL composite fibers. The fiber diameters were measured using ImageJ software (version 1.52a, NIH, USA) and the following values were obtained: 465 ± 20 μm for control scaffolds and 390 ± 51 μm for composite scaffolds. The SEM micrographs showed a well-defined porous structure, homogeneous and consistent, of the deposited scaffold structure. The scaffold morphology presented a neat spatial arrangement of pores and channels fully interconnected throughout each specimen. Nevertheless, it should be mentioned that only the composite scaffolds depicted some microstructural defects, namely, the surface roughness and shape distortion in the filaments.

TABLE 1 Melting temperature (T_m), melting enthalpy (ΔH) and crystallinity (X_c) of first and second heating scans for PCL and PCL + fG(Micrograf) scaffolds

Material	T_m (°C)	ΔH (J/g)	χ_C (%)
Scan 1			
PCL	62	90	54
PCL + fG(Micrograf)	59	92	56
Scan 2			
PCL	54	75	45
PCL + fG(Micrograf)	54	76	45

3.4 | Accelerated degradation

The degradation study performed in this work was based on the protocol proposed by Lam et al,[34,35] where a rapid degradation analysis of PCL scaffolds was made. Alkali promoted hydrolysis is similar to when degradation is made using water (or PBS), although in this situation a higher concentration of OH- is present in the solution, contributing to accelerating the degradation reaction. Figure 6 shows the scaffolds' weight loss rate for 28 days and a constant degradation rate for both control and composite scaffolds was found, suggesting that both had a similar degradation behavior. The mean original weight loss of the scaffolds was 0.075 ± 0.001 g for the control and 0.051 ± 0.001 g for the composite ones. After 28 days, it was possible to observe that PCL and PCL + fG(Micrograf) suffered a weight loss of 88.70% and 85.88%, respectively, that is, the scaffolds were almost fully degraded.

During the degradation tests, the analysis of the porosity, mean pore size and mean wall thickness was also carried out to analyze possible changes on the microstructure of the scaffold – Figure 7. The μCT images of the scaffolds were acquired along with the degradation exposure, showing the microstructure's modification of the scaffolds along time – Figure 7c. Unsurprisingly, for both scaffolds, it was observed that the porosity increased with the degradation exposure, consistently throughout the 4 weeks experienced. It reached values of approximately 90% for the control scaffolds and 83% for the composites, after 28 days of degradation. The rate of porosity increase

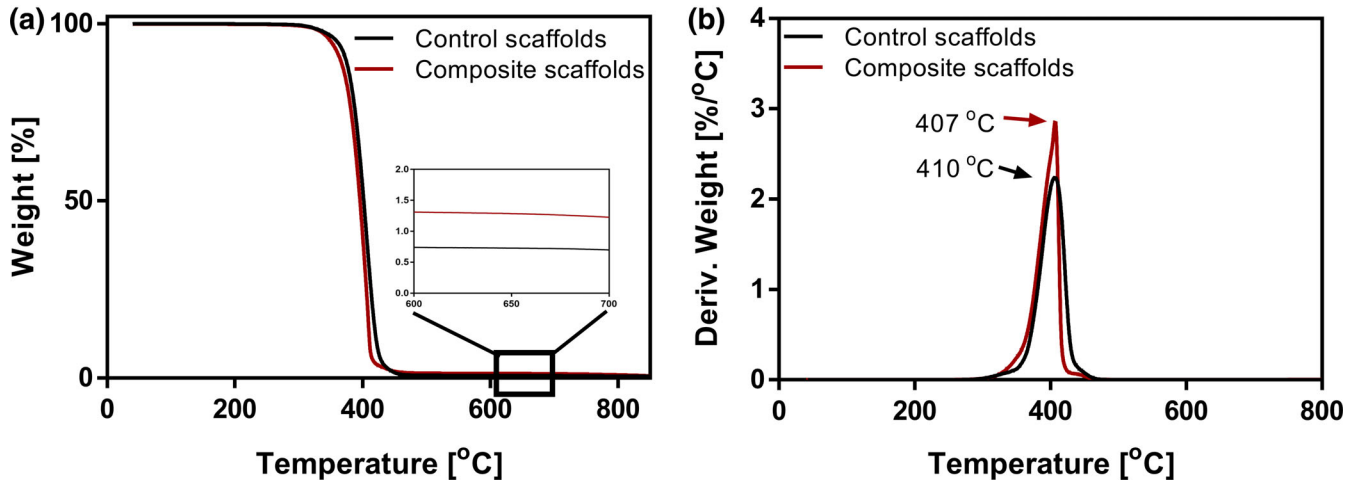

FIGURE 4 Thermogravimetric analysis of control and composite scaffolds, (a) TGA curves and (b) derivative of the weight loss curves (DTGA) for both scaffold conditions, as a function of temperature

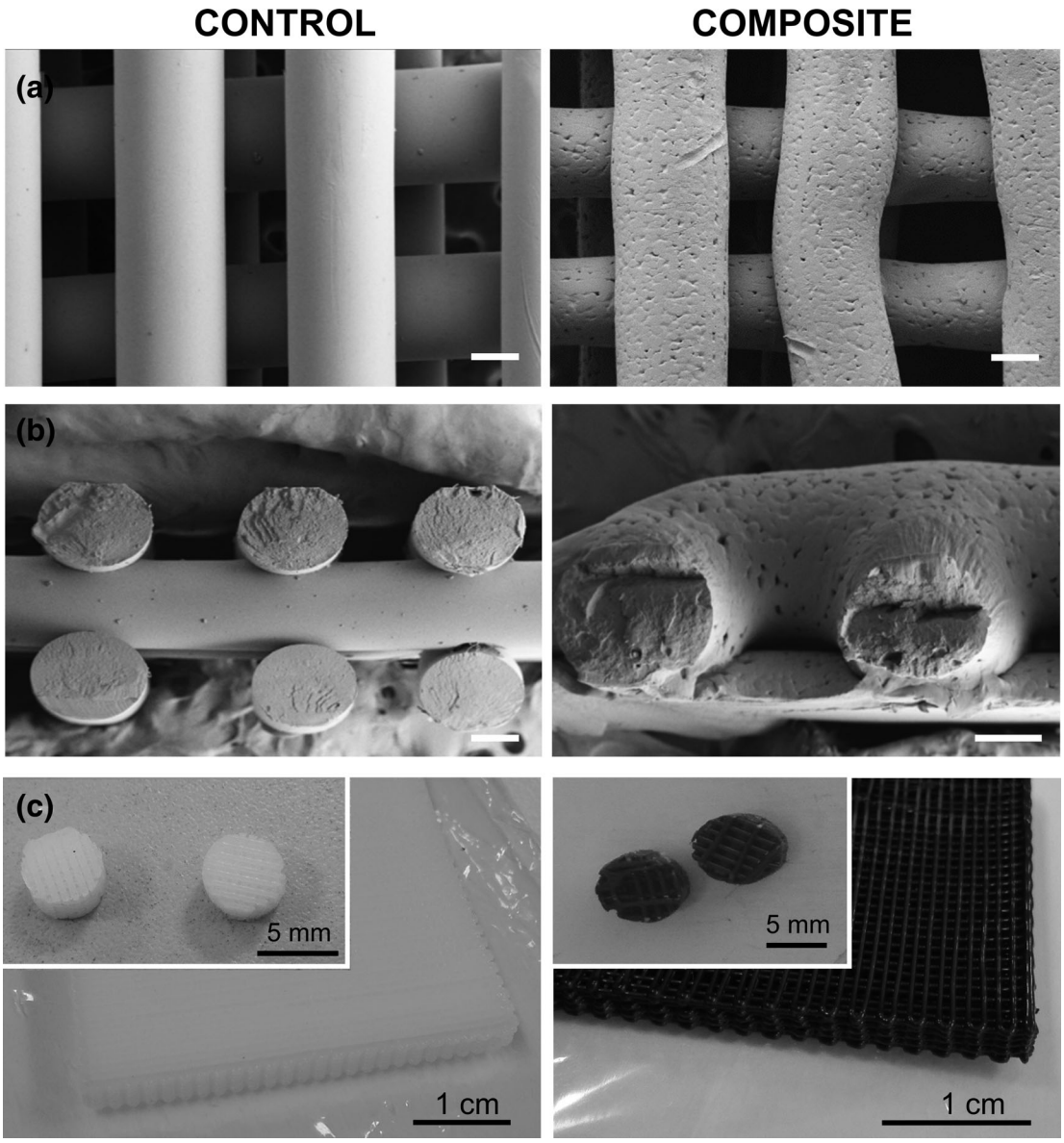

FIGURE 5 SEM images of control and composite scaffolds from (a) the top view, (b) their cross-section, where scale bars represent 200 μm; (c) and macroscopic images of the printed scaffolds and the respective cylinders cut for further characterization

was observed to be higher along the first 14 days, and fading towards the end of the degradation test, in the case of composite scaffolds. With increasing porosity, an increase in mean pore size is expected as well – Figure 7a.

At the beginning of the test, the mean pore size of the scaffolds was 322 ± 141 μm for composite scaffolds and 263 ± 103 μm for control scaffolds. Regarding the mean wall thickness measured for the fibers (Figure 7b), consistently with other microstructural parameters, the value of the wall thickness decreased with the degradation time. After 28 days of degradation, the composite scaffolds presented a mean wall thickness value of 214.95 ± 91.54 μm while the control ones presented 205.66 ± 84.96 μm. Thus, after degradation PCL + fG (Micrograf) scaffolds presented a larger wall thickness compared to PCL scaffolds, suggesting a barrier effect of fG(Micrograf) delaying the composite degradation when compared to the control one.

3.5 | Mechanical analysis

Compression tests were conducted to investigate the effect of fG(Micrograf) incorporation on the mechanical properties of PCL scaffolds – Figure 8. Representative compressive stress–strain curves are depicted in Figure 8a. It was observed that the mechanical properties of the composite samples were greatly reinforced even with a low FLG incorporation (0.5 wt%), since the compressive modulus of the scaffolds increased significantly, from 50 MPa for the control to 200 MPa for the composite (Figure 8b).

Attending the biomedical application of these scaffolds, besides compression loading, tensile tests were also performed to complementary characterize the mechanical performance of the scaffolds under tensile loading, and representative tensile stress–strain curves obtained were represented in Figure S3a, where the control scaffolds

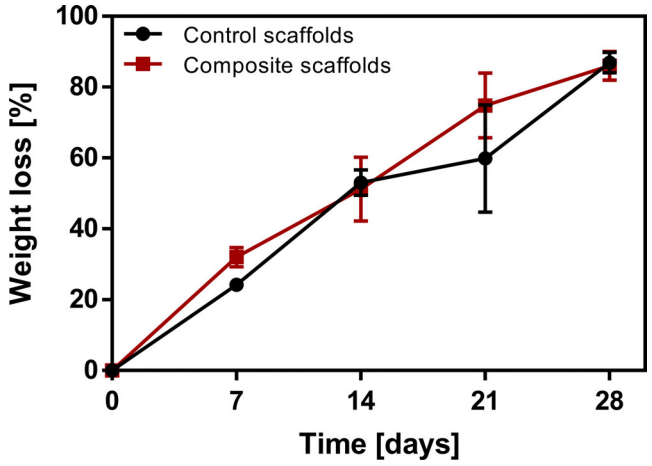

FIGURE 6 Mean percentage weight loss of control (PCL) and composite (PCL + fG(Micrograf)) scaffolds (n = 5), degraded over 4 weeks

presented slightly higher toughness than the composite ones. The determined ultimate tensile strength is plotted in Figure S3b and the tensile modulus is presented in Figure S3c, showing that the fG(Micrograf) scaffolds presented a slightly higher tensile strength and stiffness than PCL ones.

3.6 | In vitro cellular tests

Human primary osteosarcoma cell line (SaOs-2) was used to evaluate the in vitro cytotoxicity and the osteogenic differentiation ability of the produced scaffolds. The ALP activity was measured to assess the osteogenic differentiation of SaOs-2 seeded onto the PCL based scaffolds. Figure 9 shows that ALP activity of both control and composite scaffolds increased significantly from day 7 to day 14. At days 1, 3, and 7 no significant differences were stated between the two conditions, however, the ALP quantification increased over time. At

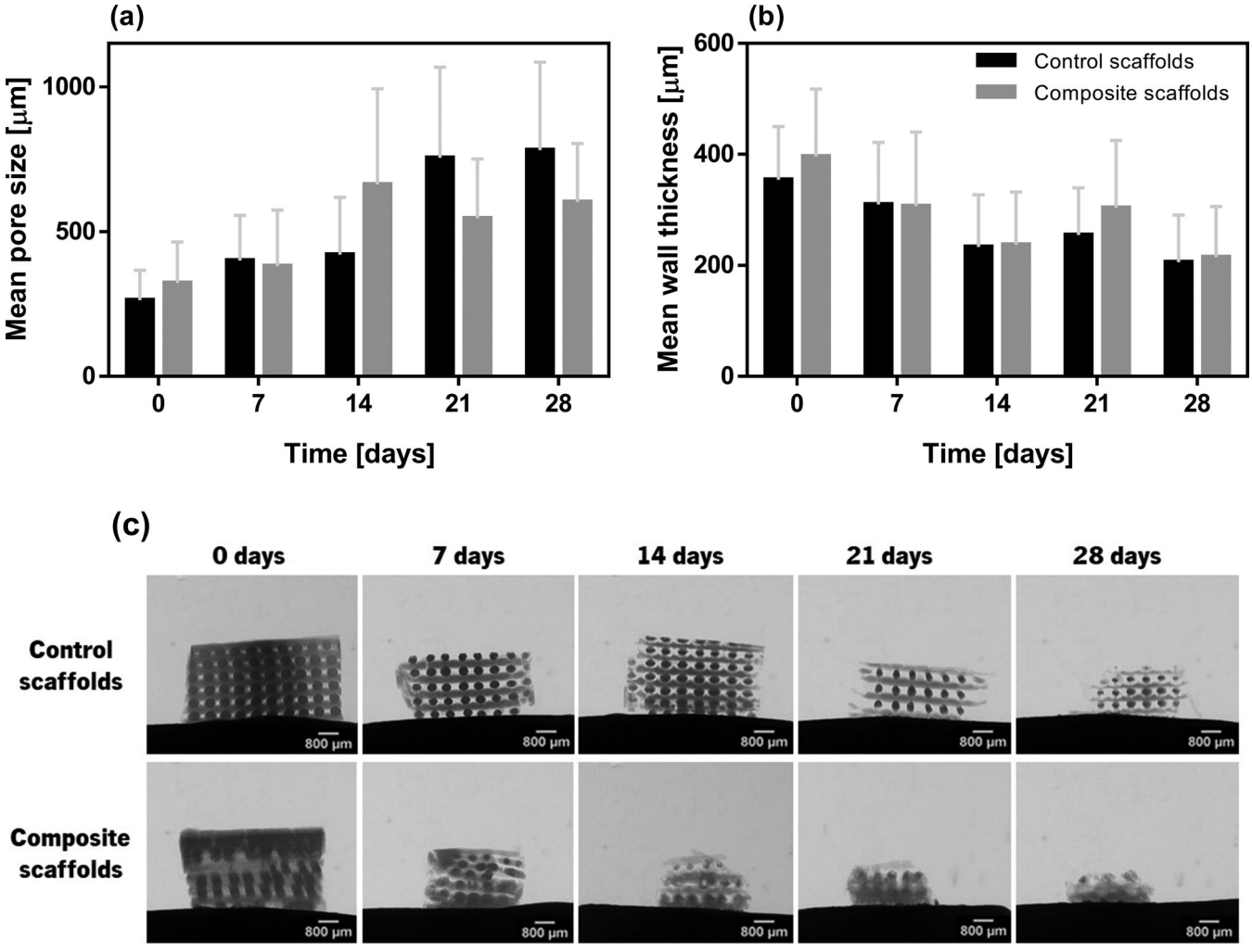

FIGURE 7 3D microstructural characterization of control and composite scaffolds, (a) mean pore size, (b) mean wall thickness, and (c) their representative μCT images during degradation tests. Scale bars represent 800 μm

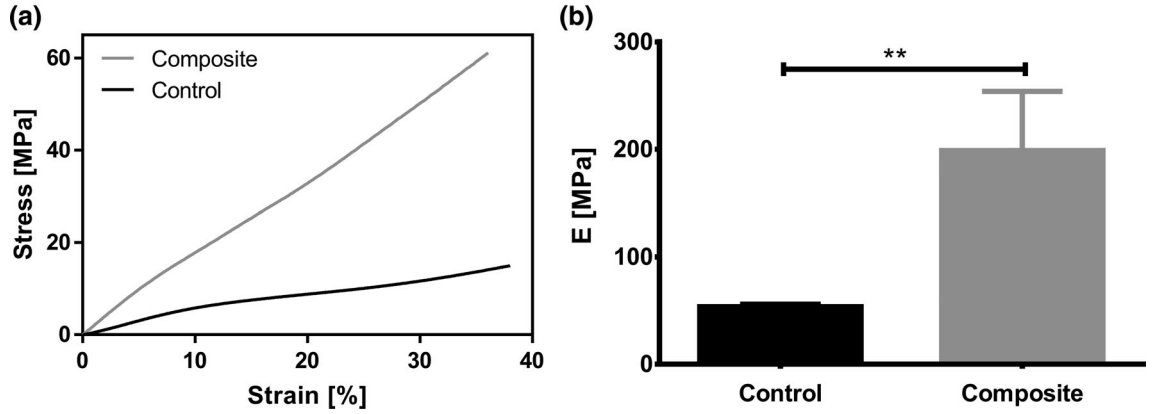

FIGURE 8 Compressive mechanical properties of control and composite scaffolds, (a) Representative stress–strain curves and (b) compressive Young's modulus, E. Statistically significant difference was found for $p < .01$ (**)

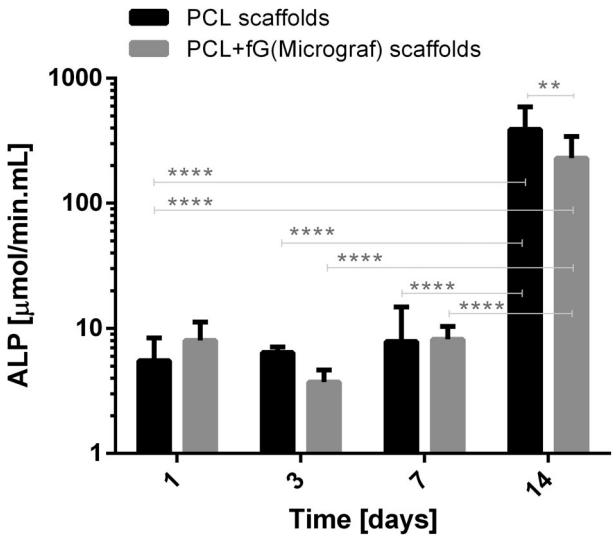

FIGURE 9 Alkaline phosphatase (ALP) activity of SaOs-2 versus incubation time performed on PCL and PCL + fG(Micrograf) scaffolds for 1, 3, 7, and 14 days. Statistically significant differences were found for $p < .01$ (**) and for $p < .0001$(****)

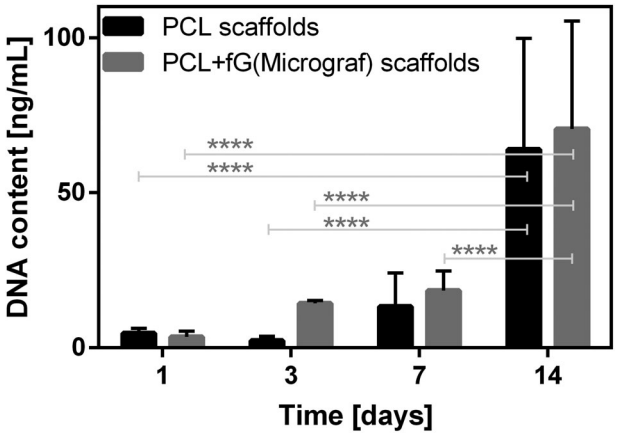

FIGURE 10 Cell proliferation through the determination of the DNA content (DNA quantification assay) performed on PCL and PCL + fG(Micrograf) scaffolds for 1, 3, 7, and 14 days. Statistically significant differences were found for $p < .0001$(****)

14 days, PCL scaffolds showed a slightly higher ALP activity when compared to PCL + fG(Micrograf) scaffolds, with a value of 389.96 µmol min^{-1} mL^{-1} against 229.28 µmol min^{-1} mL^{-1} from composites. Globally, the results showed that PCL scaffolds with or without fG(Micrograf) had very similar ALP activity values considering each time point. Regarding the cell proliferation of SaOs-2 (1, 3, 7, and 14 days) analysed on the scaffolds by assessing the DNA content, the results were presented in Figure 10. No significant differences were observed between PCL and PCL + fG(Micrograf) scaffolds until day 7. However, for the composite scaffolds, the values were slightly superior for each time point. Particularly, from day 7 to day 14, as expected, a significant increase in the DNA content was observed.

TABLE 2 Mechanical properties obtained from compressive and tensile tests for control and composite scaffolds

Material ($n = 5$)	Tensile modulus (MPa)	Compressive modulus (MPa)
Control	50.2 ± 11.6	53.6 ± 2.3
Composite	40.3 ± 5.6	198.8 ± 55.1

4 | DISCUSSION

Raman spectroscopy is one of the most used techniques for the characterization of carbon and FLG based materials. The analysis of Raman spectra in Figure 2 shows an increase in the I_D/I_G ratio from 0.13 to 0.22 after functionalization (formation of fG(Micrograf)). According to Parviz et al.,[41] this small increase might be a consequence of a decrease in the flake size when sonicating pristine Micrograf to produce fG(Micrograf). With the flake size decreasing, the

extension of exposed edges per flake rises, increasing the intensity of the D band relative to the G band. The position around 2,719 cm^{-1} and symmetric shape of the 2D band in fG(Micrograf) confirm the few-layer nature of the functionalized FLG obtained from pristine Micrograf. Pristine Micrograf was thermally stable along the temperature range analysed, as expected for pristine graphite-based materials with low contamination level, as reported by Parviz et al..[41]

From DSC analysis evaluated, it was observed that FLG incorporation did not affect the melting transition of PCL in the scaffolds (Figure 3). This may be due to the different crystallization conditions of PCL when prepared by 3D printing compared to cooling at 10°C min^{-1} from a quiescent melt.[42] Under both crystallization conditions, no differences were noted between scaffolds produced using only PCL or PCL composites incorporating FLG. These results are in agreement with a study made by Heidari et al[43] showing that the melting temperature of PCL nanofibers did not change after 1.5 wt% of FLG being incorporated in a PCL/gelatin matrix. Another study performed by Murray et al[44] has also shown that the addition of FLG did not affect the melting temperature in FLG/PCL composites. However, Diban and coworker[45] showed that the crystallinity degree of PCL-graphene oxide membranes produced by the phase inversion technique, increased when compared to PCL membranes. This was due to the nucleating effect caused by the presence of graphene oxide-based nanoplatelets in the polymer matrix, which was also responsible to increase the temperature of crystallization of the composite membranes.

Regarding the thermogravimetric analysis (Figure 4), the residual weight of PCL + fG(Micrograf) scaffolds measured at 700°C was approximately 1.22 wt%, while for the control scaffolds it was 0.69 wt%. Thereafter, the weight content of fG(Micrograf) in the scaffolds was estimated to be approximately 0.5 wt%.

The surface topography of the scaffolds was assessed by SEM and slight differences were detected in the fiber diameter from PCL and composite scaffolds. The higher deformation and plasticity of composite fibers may result from the addition of fG(Micrograf), since the addition of a small amount of graphene may have a lubricating effect on the polymer melt, reducing the melt viscosity. In fact, it was in agreement with a previous work that reported that the incorporation of a small concentration of functionalized carbon nanoparticles may considerably decrease the viscosity of the composite melt.[46] This reduction of the melt viscosity for the composite material may be interpreted as resulting from an increase in the free volume when fG(Micrograf) is dispersed in PCL. The functional groups attached to the FLG surface may increase the free volume compared to bulk PCL molecules.[46] Consequently, this lower viscosity of the composite melt may be responsible for some defects detected in the composite scaffolds (Figure 5), specifically, the surface roughness and shape distortion in the filaments. As reported in previous works,[47,48] this kind of structural defect is commonly detected in FDM-printed scaffolds and they cannot be rectified only by optimization of printing condition, being due to the nature of this printing process.[48] These drawbacks may affect the strength of the printed scaffolds, however, in the present work the mechanical performance of the composite scaffolds was not compromised.

Concerning the accelerated degradation study, as reported by Lam et al.,[34,35] the accelerated hydrolysis facilitates the study of morphological and chemical changes during degradation in a more acceptable time frame, since it has been reported that PCL presents a long-term in vivo degradation (3–4 years).[35] Herein, it was evaluated the scaffolds' weight loss rate for 28 days and, similarly with Lam et al findings,[34] a constant degradation rate for both control and composite scaffolds was found, suggesting that the addition of fG(Micrograf) did not change the degradation process of composite scaffolds in comparison with the PCL scaffolds. This progressive increase in the weight loss of the scaffolds was followed by an increase in their porosity during degradation time: starting with 36.8% for PCL and 36.3% for PCL + fG(Micrograf), and reaching 90.4% for PCL and 83.3% for PCL + fG (Micrograf) after 28 days. Effectively, the porosity is a key factor for the production of scaffolds for tissue regeneration, to enable the ingrowth and vasculature of the tissue. Hence, the developed scaffolds revealed microstructural parameters that could be suitable for tissue engineering applications, in particular, adequate porosity (<80%) and pore size (>100 μm).[49]

The compression tests showed evidence of the reinforcing effect provided by the incorporation of fG(Micrograf) in the composite scaffolds, that exhibited higher compressive modulus compared to PCL scaffolds, in agreement with previous reports. For instance, Wang et al.[50] developed 3D printed scaffolds made of PCL and pristine FLG, observing an increase in the compressive modulus from 80 to 130 MPa with the incorporation of 0.75 wt% FLG. In the present work, despite the microstructural defects detected in the filaments of composite scaffolds, the incorporation of only 0.5 wt% FLG resulted in scaffolds with higher compressive modulus, increasing from 54 to 199 MPa for PCL and composite scaffolds, respectively.

However, the incorporation of fG(Micrograf) in PCL did not lead to an improvement in tensile properties. The tensile strength was 1.6 ± 0.4 MPa for PCL scaffolds and 1.5 ± 0.4 MPa for PCL + fG (Micrograf) scaffolds and Young's modulus decreased from 50.2 ± 11.6 MPa for PCL to 40.3 ± 5.6 MPa for PCL + fG(Micrograf) scaffolds (see Table 2 and Figure S3c), but without any significant difference. In comparison with their compressive results, this lower mechanical performance of scaffolds under tensile loading could be related to the scaffold geometry implemented, a 0/90 lay-down pattern of interconnected square pores, which might be less resistant against tensile stress. Particularly, the lower tensile properties of the composite scaffolds compared to PCL scaffolds may be associated with the presence of defects in the extruded filaments, as observed by SEM. Nevertheless, similar results were presented by Song et al.[51] that found an increase in the tensile strength of PCL/graphene oxide composite scaffolds produced by electrospinning, but only for graphene oxide concentrations up to 0.3 wt%. Higher concentrations led to a decrease of the tensile strength, showing lower values compared to PCL scaffolds. Qi and co-workers[52] showed that for PVA/graphene oxide scaffolds prepared by electrospinning with 1.5–5 wt%, the tensile strength was even lower than that of pure PVA scaffolds. In agreement with these previous findings, the present

study showed that the addition of FLG to PCL could not improve the tensile properties of FLG/PCL composite scaffolds.

Finally, the preliminary cellular characterization performed confirmed the proliferation and osteoblastic differentiation of SaOs-2 cells in both structures, without cytotoxic or negative effect on the osteoblastic differentiation of the scaffolds containing fG(Micrograf). So, the incorporation of fG(Micrograf) into the PCL matrix revealed also contributes to the long-term cellular proliferation into the manufactured scaffolds.

5 | CONCLUSION

Porous degradable and non-cytotoxic PCL/fG(Micrograf) composite scaffolds were successfully prepared using the promising cryomilling technique, which enabled them to obtain homogeneous composites, printable by an extrusion-based 3D printing system.

The incorporation of non-covalently functionalized graphene, fG(Micrograf), in the composite scaffolds at approximately 0.5 wt%, was confirmed. Compression tests revealed an outstanding reinforcement effect of fG(Micrograf) in the PCL matrix, increasing by approximately four times the compressive modulus of the composite scaffolds relatively to the control. No cytotoxicity was detected for the composite scaffolds and a higher proliferation of SaOs-2 cells was observed on the composite scaffolds compared to the PCL control, suggesting adequate biological properties of FLG.

In summary, the cryomilled and 3D-printed PCL/fG(Micrograf) scaffolds exhibited enhanced compressive strength, appropriate microstructural and thermal properties, non-cytotoxicity and favorable osteoblastic differentiation ability, confirming their high potential for bone tissue engineering applications.

ACKNOWLEDGMENTS

The authors acknowledge the Portuguese Foundation for Science and Technology (FCT), the European program FEDER/COMPETE for the financial support through project LA ICVS/3Bs - 2015-2017 and to IPC (UID/CTM/50025/2013 and UID/CTM/50025/2016), and the scholarship SFRH/BD/87214/2012 granted to Eunice Cunha. Daniela Dias acknowledges the mobility grant from the BEAM project- Biomedical Engineering-EU Australian cooperation at master level, ICI-ECP Education Cooperation Programme (388414-EM-January 1, 2014-IT-ERA MUNDUS-ICIJMP). We also acknowledge Prof. Dietmar W. Hutmacher that kindly hosts Daniela Dias in the IHBI laboratory.

DATA AVAILABILITY STATEMENT

The data that support the findings of this study are available from the corresponding author upon reasonable request.

ORCID

Ana C. Vale https://orcid.org/0000-0002-1590-6636
Eunice P. F. Cunha https://orcid.org/0000-0001-8452-1783
Maria C. Paiva https://orcid.org/0000-0003-3538-5804
Natália M. Alves https://orcid.org/0000-0002-8741-4091

REFERENCES

1. Parandoush P, Lin D. A review on additive manufacturing of polymer-fiber composites. *Compos Struct*. 2017;*182*:36-53.
2. Domingos M. Effect of process parameters on the morphological and mechanical properties of 3D bioextruded poly(ε-caprolactone) scaffolds. *Rapid Prototyp J*. 2012;*18*(1):56-67.
3. Esposito Corcione C, Palumbo E, Masciullo A, Montagna F, Torricelli MC. Fused deposition modeling (FDM): an innovative technique aimed at reusing Lecce stone waste for industrial design and building applications. *Const Build Mater*. 2018;*158*:276-284.
4. Yun P-Y. The application of three-dimensional printing techniques in the fi eld of oral and maxillofacial surgery. *J Korean Assoc Oral Maxillofac Surg*. 2015;*41*(4):169-170.
5. Xie H, Cao T, Rodríguez-Lozano FJ, Luong-Van EK, Rosa V. Graphene for the development of the next-generation of biocomposites for dental and medical applications. *Dent Mater*. 2017;*33*(7):765-774.
6. Bedian L, Villalba-Rodriguez AM, Hernandez-Vargas G, Parra-Saldivar R, Iqbal HM. Bio-based materials with novel characteristics for tissue engineering applications - a review. *Int J Biol Macromol*. 2017;*98*:837-846.
7. Gunatillake PA, Adhikari R. Biodegradable synthetic polymers for tissue engineering. *Eur Cell Mater*. 2003;*5*:1-16.
8. Holt BD, Wright ZM, Arnold AM, Sydlik SA. Graphene oxide as a scaffold for bone regeneration. *Wiley Interdiscip Rev Nanomed Nanobiotechnol*. 2017;*9*(3):e1437.
9. Yoshimoto H, Shin YM, Terai H, Vacanti JP. A biodegradable nanofiber scaffold by electrospinning and its potential for bone tissue engineering. *Biomaterials*. 2003;*24*(12):2077-2082.
10. Mondal D, Griffith M, Venkatraman SS. Polycaprolactone-based biomaterials for tissue engineering and drug delivery: current scenario and challenges. *Int J Polym Mater Polym Biomater*. 2016;*65*(5):255-265.
11. Dash TK, Konkimalla VB. Poly-small je, Ukrainian-caprolactone based formulations for drug delivery and tissue engineering: a review. *J Control Release*. 2012;*158*(1):15-33.
12. Avouris P, Dimitrakopoulos C. Graphene: synthesis and applications. *Mater Today*. 2012;*15*(3):86-97.
13. Cunha EPF. Functionalized graphene for polymer composites [Doctoral Thesis (Ciência e Engenharia de Polímeros e Compósitos)]: University of Minho; 2016. p. 206.
14. Dasari BL, Nouri JM, Brabazon D, Naher S. Graphene and derivatives – synthesis techniques, properties and their energy applications. *Energy*. 2017;*140*:766-778.
15. Shin SR, Li Y-C, Jang HL, et al. Graphene-based materials for tissue engineering. *Adv Drug Deliv Rev*. 2016;*105*:255-274.
16. Tyona MD. A theoritical study on spin coating technique. *Adv Mater Res*. 2013;*2*:195-208.
17. Sayyar S, Officer DL, Wallace GG. Fabrication of 3D structures from graphene-based biocomposites. *J Mater Chem B*. 2017;*5*(19):3462-3482.
18. Georgakilas V, Otyepka M, Bourlinos AB, et al. Functionalization of graphene: covalent and non-covalent approaches, derivatives and applications. *Chem Rev*. 2012;*112*(11):6156-6214.
19. Xu Z, Wang S, Li Y, Wang M, Shi P, Huang X. Covalent functionalization of graphene oxide with biocompatible poly(ethylene glycol) for delivery of paclitaxel. *ACS Appl Mater Interfaces*. 2014;*6*(19):17268–17276.
20. Singh NJ, Lee HM, Hwang I-C, Kim KS. Designing Ionophores and molecular nanotubes based on molecular recognition. *Supramol Chem*. 2007;*19*(4–5):321-332.

21. Georgakilas V, Tiwari JN, Kemp KC, et al. Noncovalent functionalization of graphene and graphene oxide for energy materials, biosensing, catalytic, and biomedical applications. *Chem Rev*. 2016;*116*(9):5464-5519.
22. Cunha E, Proença MF, Pereira MG, et al. Water dispersible few-layer graphene stabilized by a novel pyrene derivative at micromolar concentration. *Nanomaterials*. 2018;*8*(9):675.
23. Allaf RM, Rivero IV. Fabrication and characterization of interconnected porous biodegradable poly(ε-caprolactone) load bearing scaffolds. *J Mater Sci Mater Med*. 2011;*22*(8):1843-1853.
24. Mukhopadhyay P, Gupta RK. *Graphite, graphene, and their polymer nanocomposites*. Vol 631, 6000 Broken Sound Parkway NW, Boca Raton, USA: CRC Press; 2013.
25. Wang W, Caetano G, Ambler WS, et al. Enhancing the hydrophilicity and cell attachment of 3D printed PCL/graphene scaffolds for bone tissue engineering. *Materials*. 2016;*9*:992.
26. Chen Q, Mangadlao JD, Wallat J, De Leon A, Pokorski JK, Advincula RC. 3D printing biocompatible polyurethane/poly(lactic acid)/graphene oxide nanocomposites: anisotropic properties. *ACS Appl Mater Interfaces*. 2017;*9*(4):4015-4023.
27. Unagolla JM, Jayasuriya AC. Hydrogel-based 3D bioprinting: a comprehensive review on cell-laden hydrogels, bioink formulations, and future perspectives. *Appl MaterToday*. 2020;*18*:100479.
28. Feng Z, Li Y, Hao L, et al. Graphene-reinforced biodegradable resin composites for stereolithographic 3D printing of bone structure scaffolds. *J Nanomater*. 2019;*2019*:9710264.
29. Rajzer I, Kurowska A, Jabłoński A, et al. Scaffolds modified with graphene as future implants for nasal cartilage. *J Mater Sci*. 2020;*55*(9):4030-4042.
30. Bas O, Hanßke F, Lim J, et al. Tuning mechanical reinforcement and bioactivity of 3D printed ternary nanocomposites by interfacial peptide-polymer conjugates. *Biofabrication*. 2019;*11*(3):035028.
31. Domingos M, Dinucci D, Cometa S, Alderighi M, Bártolo PJ, Chiellini F. Polycaprolactone scaffolds fabricated via Bioextrusion for tissue engineering applications. *Int J Biomater*. 2009;*2009*:239643.
32. Domingos M, Chiellini F, Cometa S, et al. Evaluation of in vitro degradation of PCL scaffolds fabricated via BioExtrusion – part 2: influence of pore size and geometry. *Virt Phys Prototyp*. 2011;*6*(3):157-165.
33. Malheiro VN, Caridade SG, Alves NM, Mano JF. New poly(epsilon-caprolactone)/chitosan blend fibers for tissue engineering applications. *Acta Biomater*. 2010;*6*(2):418-428.
34. Lam CX, Savalani MM, Teoh SH, Hutmacher DW. Dynamics of in vitro polymer degradation of polycaprolactone-based scaffolds: accelerated versus simulated physiological conditions. *Biomed Mater*. 2008;*3*(3):034108.
35. Lam CX, Teoh SH, Hutmacher DW. Comparison of the degradation of polycaprolactone and polycaprolactone–(β-tricalcium phosphate) scaffolds in alkaline medium. *Polym Int*. 2007;*56*(6):718-728.
36. Mano JF, Silva GA, Azevedo HS, et al. Natural origin biodegradable systems in tissue engineering and regenerative medicine: present status and some moving trends. *J Royal Soc Interfaces*. 2007;*4*(17):999-1030.
37. Zhu Y, Murali S, Cai W, et al. Graphene and graphene oxide: synthesis, properties, and applications. *Adv Mater*. 2010;*22*(35):3906-3924.
38. Ni Z, Wang Y, Yu T, Shen Z. Raman spectroscopy and imaging of graphene. *Nano Res*. 2008;*1*(4):273-291.
39. Wang Y, Ni Z, Yu T, et al. Raman studies of monolayer graphene: the substrate effect. *J Phys Chem C*. 2008;*112*(29):10637–10640.
40. Ferrari AC, Basko DM. Raman spectroscopy as a versatile tool for studying the properties of graphene. *Nat Nanotech*. 2013;*8*(4):235-246.
41. Parviz D, Das S, Ahmed HST, Irin F, Bhattacharia S, Green MJ. Dispersions of non-covalently functionalized graphene with minimal stabilizer. *ACS Nano*. 2012;*6*(10):8857-8867.
42. Sanandaji N. Different paths to explore confined crystallisation of PCL [Doctoral Thesis]. Stockholm: KTH Royal Institute of Technology; 2013. p. 72.
43. Heidari M, Bahrami H, Ranjbar-Mohammadi M. Fabrication, optimization and characterization of electrospun poly(caprolactone)/gelatin/graphene nanofibrous mats. *Mater Sci Eng C*. 2017;*78*:218-229.
44. Murray E, Thompson BC, Sayyar S, Wallace GG. Enzymatic degradation of graphene/polycaprolactone materials for tissue engineering. *Polym Degrad Stab*. 2015;*111*:71-77.
45. Diban N, Sánchez-González S, Lázaro-Díez M, Ramos-Vivas J, Urtiaga A. Facile fabrication of poly(ε-caprolactone)/graphene oxide membranes for bioreactors in tissue engineering. *J Memb Sci*. 2017;*540*:219-228.
46. Martins JA, Cruz VS, Paiva MC. Flow activation volume in composites of polystyrene and multiwall carbon nanotubes with and without functionalization. *Macromolecules*. 2011;*44*(24):9804-9813.
47. Wickramasinghe S, Do T, Tran P. FDM-based 3D printing of polymer and associated composite: a review on mechanical properties, defects and treatments. *Polymers*. 2020;*12*(7):1529.
48. Oztan C, Karkkainen R, Fittipaldi M, et al. Microstructure and mechanical properties of three dimensional-printed continuous fiber composites. *J Compos Mater*. 2018;*53*(2):002199831878193.
49. Karageorgiou V, Kaplan D. Porosity of 3D biomaterial scaffolds and osteogenesis. *Biomaterials*. 2005;*26*(27):5474-5491.
50. Wang WG, Chang WH, Bartolo PJ. Design, fabrication and evaluation of pcl/graphene scaffolds for bone regeneration. In: C.K. Chu WLY, M.J. Tan, E. Liu, S.B. Tor, eds. Proc. of the 2nd Intl. Conf. On Progress in additive manufacturing. Singapore: Research Publishing; 2016. pp. 355–360.
51. Song J, Gao H, Zhu G, Cao X, Shi X, Wang Y. The preparation and characterization of polycaprolactone/graphene oxide biocomposite nanofiber scaffolds and their application for directing cell behaviors. *Carbon*. 2015;*95*:1039-1050.
52. Qi YY, Tai ZX, Sun DF, et al. Fabrication and characterization of poly(vinyl alcohol)/graphene oxide nanofibrous biocomposite scaffolds. *J Appl Polym Sci*. 2013;*127*(3):1885-1894.

SUPPORTING INFORMATION

Additional supporting information may be found online in the Supporting Information section at the end of this article.

How to cite this article: Dias D, Vale AC, Cunha EPF, et al. 3D-printed cryomilled poly(ε-caprolactone)/graphene composite scaffolds for bone tissue regeneration. *J Biomed Mater Res*. 2020;1–12. https://doi.org/10.1002/jbm.b.34761